Article



SANS reveals lipid-dependent oligomerization of an intramembrane aspartyl protease from *H. volcanii*

Gwendell M. Thomas, ¹ Yuqi Wu, ¹ Wellington Leite, ² Sai Venkatesh Pingali, ² Kevin L. Weiss, ² Arshay J. Grant, ³ Monneh W. Diggs, ³ Ingeborg Schmidt-Krey, ^{1,3} Gvantsa Gutishvili, ⁴ James C. Gumbart, ^{1,4} Volker S. Urban, ^{2,*} and Raguel L. Lieberman^{1,*}

¹School of Chemistry & Biochemistry, Georgia Institute of Technology, Atlanta, Georgia; ²Neutron Scattering Division, Oak Ridge National Laboratory, Oak Ridge, Tennessee; ³School of Biological Sciences, Georgia Institute of Technology, Atlanta, Georgia; and ⁴School of Physics, Georgia Institute of Technology, Atlanta, Georgia

ABSTRACT Reactions that occur within the lipid membrane involve, at minimum, ternary complexes among the enzyme, substrate, and lipid. For many systems, the impact of the lipid in regulating activity or oligomerization state is poorly understood. Here, we used small-angle neutron scattering (SANS) to structurally characterize an intramembrane aspartyl protease (IAP), a class of membrane-bound enzymes that use membrane-embedded aspartate residues to hydrolyze transmembrane seqments of biologically relevant substrates. We focused on an IAP ortholog from the halophilic archaeon Haloferax volcanii (HvoIAP). HvoIAP purified in n-dodecyl-β-D-maltoside (DDM) fractionates on size-exclusion chromatography (SEC) as two fractions. We show that, in DDM, the smaller SEC fraction is consistent with a compact HvoIAP monomer. Molecular dynamics flexible fitting conducted on an AlphaFold2-generated monomer produces a model in which loops are compact alongside the membrane-embedded helices. In contrast, SANS data collected on the second SEC fraction indicate an oligomer consistent with an elongated assembly of discrete HvolAP monomers. Analysis of in-line SEC-SANS data of the HvolAP oligomer, the first such experiment to be conducted on a membrane protein at Oak Ridge National Lab (ORNL), shows a diversity of elongated and spherical species, including one consistent with the tetrameric assembly reported for the Methanoculleus marisnigri JR1 IAP crystal structure not observed previously in solution. Reconstitution of monomeric HvolAP into bicelles increases enzyme activity and results in the assembly of HvolAP into a species with similar dimensions as the ensemble of oligomers isolated from DDM. Our study reveals lipid-mediated HvolAP self-assembly and demonstrates the utility of in-line SEC-SANS in elucidating oligomerization states of small membrane proteins.

SIGNIFICANCE How lipids regulate membrane-bound enzyme activity is poorly understood but can be probed by neutron scattering experiments in solution. Here, we studied how lipids affect the oligomerization state of an intramembrane aspartyl protease from *H. volcanii*. We show that lipids promote the assembly of *H. volcanii* IAP into higher-order oligomers. We also introduce a new in-line size-exclusion chromatography small-angle neutron scattering experiment at the ORNL beamline.

INTRODUCTION

Proteolysis within the lipid membrane requires a quaternary complex composed of an intramembrane protease (IP), a transmembrane segment of a substrate, a lipid membrane,

Submitted January 16, 2024, and accepted for publication May 29, 2024. *Correspondence: urbanvs@ornl.gov or raquel.lieberman@chemistry.gatech.edu

Gwendell M. Thomas, Yuqi Wu, and Wellington Leite contributed equally to this work

Editor: Frederick Heberle.

https://doi.org/10.1016/j.bpj.2024.05.029

© 2024 Biophysical Society.

and bulk water. IPs underlie major biological pathways such as immune response and surveillance, cholesterol biosynthesis, and other signaling pathways in the cell (1). However, molecular details of how the various components work in concert to perform hydrolysis at the right time and place remain poorly understood.

Even the most basic characterization, such as the oligomeric state of a catalytically active IP, remains unclear. For example, evidence for monomer (2), dimer (3–5), and tetramer (6–8) has been put forth for the subject of this study, the intramembrane aspartyl protease (IAP) family, where two catalytic aspartates are used for hydrolysis in



the membrane. The archetypal members of the IAP family are signal peptide peptidase and presenilin, the latter of which is found in the heterooligomeric, γ-secretase complex associated with Alzheimer's disease (9). Determining the oligomeric state of membrane proteins such as IAPs is challenging by standard biophysical and biochemical methodology due to the presence of detergent in the purification buffers, which is required to retain the native enzyme in solution. To underscore the importance of oligomerization, for human signal peptide peptidase, different states are proposed to be responsible for differential functions in the cell, either cleaving signal peptides for nascent protein maturation or degrading protein as part of endoplasmicreticulum-associated degradation (10). In addition, for γ-secretase, super-resolution microscopy indicates both monomers and dimers of the four-component system are seen, depending on the specific cellular membrane imaged (11).

Lipid mimics are required for studies of membrane proteins and, of these, bicelles (12) are a convenient choice. Bicelles composed of 1,2-dimyristoyl-sn-glycero-3-phosphocholine (DMPC) and 3-[(3-cholamidopropyl)dimethylammino]-2hydroxy-1-propanesulfonate (CHAPSO) are fluid miscible with proteins in solution at low temperature, whereas their consistency changes to a gel at higher temperature. Characterization of DMPC/CHAPSO bicelles by our labs (13) using small-angle neutron scattering (SANS) shows how the nanoscale morphology of the lipid changes as a function of temperature. At low temperatures, bicelles form membranebilayer-like discs, whereas, at higher temperatures, bicelles form cylindrical ribbons of significant length (>3000 Å). This finding raises the question of what happens to a membrane protein embedded in a bicelle as a function of temperature.

Here, we use SANS to study bicelle-dependent protein oligomerization, focusing on an IAP ortholog from the halophile H. volcanii (HvoIAP) (UniProt: A0A8T5CT58, GenBank: WP_004043830.1). Recombinant expression of HvoIAP in E. coli yields high levels of protein including conditions yielding perdeuterated protein for SANS, which is required to enhance the scattering signal of this small membrane enzyme. HvoIAP purified in n-dodecyl-β-D-maltoside (DDM) fractionates by size-exclusion chromatography (SEC) into two main species. SANS data show that the fractionated HvoIAP species are best described as a compact monomer and an oligomer forming an elongated cylinder. In-line SEC-SANS experiments, the first such experiments conducted on a membrane protein at Oak Ridge National Lab (ORNL), reveal that the oligomeric fraction is composed of a multitude of assemblies, the smallest species of which is consistent with a tetramer. Our study demonstrates a role for lipids in the self-assembly of membrane enzymes that correlates with enzyme activity as well as the utility of SEC-SANS in detecting different oligomeric species of small membrane proteins in solution.

MATERIALS AND METHODS

Expression and purification of protiated HvoIAP

A codon-optimized gene corresponding to wild type (WT) HvoIAP WT was cloned into a pET-22b(+) vector by BioBasic. The plasmid encodes an N-terminal pelB leader sequence for periplasmic membrane insertion and a C-terminal hexahistidine tag for affinity purification. Plasmid fidelity was confirmed by DNA sequencing (Eton). HvoIAP expression and purification were adapted from previously established methods for Methanoculleus marisnigri JR1 (MmIAP) (14,15). A plasmid containing WT HvoIAP was transformed into E. coli Rosetta 2 (DE3) cells (Novagen, Madison, WI). Single colonies were selected and grown overnight in 100 mL cultures of LB medium with 34 μg/mL chloramphenicol and 60 μg/mL ampicillin at 37°C. Large cultures (1 L each) were inoculated with overnight inoculum and grown in LB medium with 34 μ g/mL chloramphenicol and 60 μ g/mL ampicillin in an orbital shaker (225 rpm, 37°C) until OD₆₀₀ of 1.5-1.8 was reached. The cultures were cooled to 22°C for 1 h, and protein expression was induced by 0.2 mM isopropyl-β-D-1-thiogalactopyranoside (IPTG). Cultures were grown overnight, harvested by centrifugation at $5000 \times g$, flashcooled with liquid nitrogen, and stored at -80° C.

For membrane isolation, 6.5 g of frozen cell paste was thawed and suspended in 35 mL cell resuspension buffer (50 mM HEPES, 200 mM NaCl [pH 7.5]) containing Complete EDTA-free protease inhibitor cocktail (Roche, Basel, Switzerland). The cell suspension was lysed by a French press twice at 12,000 psi and centrifuged at $5000 \times g$ for 45 min to remove cell debris. The supernatant was ultracentrifuged at $162,000 \times g$ for 30 min. The pelleted membrane fraction was washed in fresh cell resuspension buffer using a Dounce homogenizer. The membrane fraction was pelleted again by ultracentrifugation at $162,000 \times g$ for 30 min.

For purification, 0.5 g of wet membranes was solubilized in 40 mL of 50 mM HEPES, 500 mM NaCl, 20 mM imidazole (pH 7.5), and 1% (w/v) DDM (Anatrace, Maumee, OH) by gentle rocking for 1 h at 4°C. The sample was ultracentrifuged at $162,000 \times g$ for 30 min. The supernatant containing solubilized membranes was purified by a 1 mL HisTrap FF column (Cytiva, Marlborough, MA) on an ÄKTA Pure chromatography system (Cytiva). The column was equilibrated in buffer A (50 mM HEPES, 500 mM NaCl, 20 mM imidazole [pH 7.5], 0.1% DDM) and proteins were eluted by a linear gradient from 0% to 60% buffer B (50 mM HEPES, 500 mM NaCl, 500 mM imidazole [pH 7.5], 0.1% DDM). Elution fractions were pooled, and buffer exchanged into PBS (10 mM Na₂HPO₄/KH₂PO₄, 150 mM NaCl [pH 7.2]) with 0.05% DDM in Amicon Ultra 15 mL centrifugal filter units (Millipore, Burlington, MA) with a molecular weight cut-off (MWCO) of 50 kDa. The sample was concentrated to $\sim 900~\mu L$ and subjected to HiPrep 16/60 Sephacryl S-300 HR or Sephacryl S-200 Increase GL 100/300 columns (Cytiva) using the same PBS buffer (0.05% DDM) at 4°C. Purity was assessed by 12% SDS-PAGE analysis visualized by standard Coomassie staining. Fractions of interest were pooled and concentrated using Amicon Ultra 15 mL centrifugal filter units (Millipore) with a 50 kDa MWCO. For samples in bicelles, after concentration, the sample was reconstituted into 5% (w/v) DMPC/CHAPSO bicelles (2.8:1 M ratio, 3 mass ratio) (16) by diluting a 25% bicelle stock with protein and buffer to the desired final concentrations in 5% bicelles and incubating the samples on ice for >1 h, as described previously (14). The concentration of HvoIAP was calculated from Beer's law using absorbance at 280 nm and an extinction coefficient calculated from ExPASy Prot-Param (17).

Enzyme activity assay

We measured HvoIAP activity in an established gel assay using a substrate containing the leader sequence from the tyrosine receptor kinase ErbB4 (14). In brief, the sequence LVIVGLTFAV was inserted in between the sequence for maltose binding protein and yeast small ubiquitin-like modifier followed by a hexahistidine tag, and the fusion substrate expressed and purified as described previously (14). Freshly purified HvoIAP (16 μM) in either DDM or reconstituted into bicelles was incubated with substrate (5 μ M) at 37°C for 48 h. The assay buffer was 20 mM HEPES (pH 7.5), 2 M KCl. At each time point, 10 µL of the reaction mixture was taken and quenched by an equal volume of 2× Laemmli sample buffer. At the conclusion of the experiments, western blot analysis of each time point was conducted. Samples were separated on 12% SDS-PAGE gel with a PageRuler Plus Pre-Stained Protein Ladder (Thermo Fisher Scientific, Waltham, MA) and transferred onto a PVDF membrane via the Trans-Blot Turbo Transfer System (Bio-Rad, Hercules, CA). The primary antibody to detect maltose binding protein was mouse monoclonal IgG (1:1000, Santa Cruz Biotchnhology, Dallas, TX) and the secondary antibody used was HRP-conjugated goat anti-mouse monoclonal IgG (KPL, 1:5000 dilution, Thermo Fisher Scientific). The membrane was incubated with Denville Hyglo spray (Thomas Scientific, Logan Township, NJ) and visualized using a ChemiDoc Imaging System (Bio-Rad). Data presented are representative of at least two biological replicates.

Expression and purification of deuterated HvoIAP

To express partially deuterated HvoIAP (d-HvoIAP), a shaker-flask growth protocol (18) was first optimized for yield, with the highest yield obtained with the following protocol. A starter culture (25 mL in LB broth) was grown as for protiated HvoIAP overnight, and then cells were centrifuged at 5000 \times g for 10 min. The pellet was resuspended in 25 mL fresh LB medium and used to inoculate four 1 L cultures in LB medium with 34 µg/mL chloramphenicol and 60 μ g/mL carbenicillin. The cells were incubated in an orbital shaker (225 rpm, $37^{\circ}\text{C})$ until OD_{600} of 1.6–1.8 was reached. The cultures were centrifuged at $5000 \times g$ for 10 min in presterilized centrifuge bottles. Each pellet was washed in Enfors (19) minimal medium (7 g/L (NH₄)₂SO₄, 5.25 g/L Na₂HPO₄, 1.6 g/L KH₂PO₄, 0.5 g/L citric acid ammonium salt, 5 g/L glycerol, 1.0 mL/L 20% [w/v] MgSO₄·7H₂O, 1 mL/L Holme trace elements [0.5 g/L CaCl2·H2O, 0.098 g/L CoCl2, 0.102 g/L CuSO₄, 16.7 g/L FeCl₃·6H₂O, 0.114 g/L MnSO₄·H₂O, 22.3 g/L Na₂EDTA·2H₂O, 0.112 g/L ZnSO₄·H₂O]) (20) prepared in 75% D₂O, repelleted by centrifugation at 5000 × g for 10 min, and resuspended in 250 mL 75% D₂O Enfors minimal medium in 2.8 L Fernbach flasks. The cultures were grown at 22°C for 1 h before being induced by 0.2 mM IPTG for 48 h. Cells were harvested by centrifugation at 5000 \times g, flash frozen with liquid nitrogen, and stored at -80°C. Membrane isolation was performed the same way as for protiated HvoIAP (h-HvoIAP). For the SANS experiment characterizing the putative monomer in DDM, d-HvoIAP was purified with the same process as h-HvoIAP with the following modifications to account for the increased scale of membrane to account for the overall lower expression. Each purification was initially scaled 5-fold and the process repeated a total of three times. Specifically, ~2.5 g membrane was solubilized in 200 mL buffer and the affinity purification was scaled to a 5 mL HisTrap FF column (Cytiva) before fractionating on a Sephacryl S-300 SEC column. Three rounds of solubilization, affinity chromatography, and SEC were conducted to purify d-HvoIAP from a total of 7.5 g of membranes. Fractions of interest (putative oligomer and monomer, see results) from each of the three SEC runs were pooled and subjected again to SEC on a Sephacryl S-300 column. Per our contrast matching protocol, the putative monomer fractions were pooled, concentrated using Amicon Ultra 15 mL centrifugal filter units (Millipore) with a 50 kDa MWCO, and loaded onto a Superose-12 10/300 GL (Cytiva) SEC column equilibrated with 20 mM HEPES, 250 mM NaCl (pH 7.5), 48.5% D₂O, and 0.05% DDM (composed of 44% [w/v] tail-deuterated d₂₅-DDM [Anatrace]). The d-HvoIAP sample was concentrated to \sim 400 μ L using a 50 kDa MWCO 15 mL Amicon concentrator. A blank sample buffer was concentrated in the same fashion. The final yield of purified putatively monomeric HvoIAP was ~ 1 mg from a 7.5 mg membrane, originating from 4 L E. coli cell culture.

For SANS experiments to characterize the putative d-HvoIAP monomer reconstituted into bicelles, the membrane was solubilized and purified through the final polishing S-300 SEC step as above. After concentrating the sample, half of the sample was loaded onto a Superose-12 column equilibrated with 20 mM HEPES, 250 mM NaCl (pH 7.5), 15% D₂O, and the other half was loaded on the column after equilibration with 20 mM HEPES, 250 mM NaCl (pH 7.5), 21% D₂O. The elution peaks from each respective run were pooled and concentrated using Amicon Ultra 15 mL centrifugal filter units (Millipore) with a 50 kDa MWCO. The sample in 15% D₂O was reconstituted into 5% DMPC/CHAPSO bicelles (16) prepared as described previously (14), whereas the sample in 21% D₂O was reconstituted into 5% DMPC/CHAPSO bicelles in which 18% (w/v) of DMPC was tail-deuterated d₅₄-DMPC. Reconstitution proceeded by incubating samples on ice for >1 h. For each sample, a buffer blank was concentrated and reconstituted into the bicelle mixture in the same way.

For SANS experiments to characterize the putative d-HvoIAP oligomer species in DDM, the associated fractions from three S-300 chromatograms were pooled and polished on the S-300. The purified oligomer fractions were pooled and loaded onto a Superose-12 column equilibrated with 20 mM HEPES, 250 mM NaCl (pH 7.5), 48.5% D₂O, and 0.05% DDM, of which 44% (w/v) is tail-deuterated $d_{25}\mbox{-}DDM$ (Anatrace) per our contrast matching protocol. The final yield of purified putatively oligomeric HvoIAP was ~2.8 mg from 7.5 mg membrane derived from 4 L culture, with final samples for SANS prepared at ~2.5 mg/mL. A buffer blank was concentrated in the same fashion.

SANS data collection

SANS data were collected at the Bio-SANS instrument (21,22) on beamline CG-3 of the High-Flux Isotope Reactor at ORNL (23). SANS experiments for all samples except the d-HvoIAP oligomer in DDM used a single instrument configuration of the dual detector system, the flat main detector at 15.5 m from sample and the curved wing detector at an angle of 1.4° with respect to the main beam. The Panel Scan feature of the data acquisition system was used to control the instrument during measurement. In this configuration, the range of momentum transfer values (Q) was $0.003 < Q < 1 \ \mathring{A}^{-1},$ where $Q = 4\pi \, \cdot \, sin(\theta) \! / \! \lambda$ (20 is the scattering angle and λ is the neutron wavelength). Neutrons with a wavelength of 6 Å and a relative wavelength spread ($\Delta\lambda\lambda$) of 13.2% were utilized. SANS samples were loaded in 1 mm pathlength cylindrical quartz cuvettes (Hellma, Müllheim, Germany) and measured. The putative d-HvoIAP monomer in DDM, d-HvoIAP oligomer in DDM, and empty DDM micelles background were measured at 48.5% D₂O (contrast match point of mixed DDM and d₂₅-DDM micelles) and at 10°C maintained by a Peltier temperature control. d-HvoIAP monomer in DMPC/CHAPSO bicelles and empty bicelles background were measured at 15% D₂O (contrast match point of bicelles) and at 10°C. Buffer blanks were subtracted from the sample scattering for background correction. The processed scattering data were circularly averaged and reduced to 1D scattering profiles using MantidPlot software (24). Calibration of the SANS data to an absolute scale was performed by measuring a porous silica standard with known intensity at zero angle (extrapolated from a Debye-Bueche plot).

The SANS experiment for d-HvoIAP oligomer in DDM used the configuration with the main detector at 7 m and the curved wing detector at 3.2°. In this configuration, the range of momentum transfer (Q) was $0.007 < Q < 1 \text{ Å}^{-1}$. Neutrons with a wavelength of 6 Å and a relative wavelength spread ($\Delta \lambda / \lambda$) of 13.2% were utilized.

SEC-SANS

SEC-SANS was carried out at room temperature using a modified ÄKTA Pure 25 protein purification system (Cytiva) equipped with multiwavelength detection, a DEGASi Plus Micro degasser (Biotech), an ALIAS Bio Cool autosampler (Cytiva), and a Superdex 200 Increase 10/300 column (Cytiva). The column was equilibrated with two column volumes of buffer consisting of 10 mM sodium phosphate (pH 7.4), 150 mM NaCl, and 0.05% total DDM in 49% D2O. To enable contrast matching, the

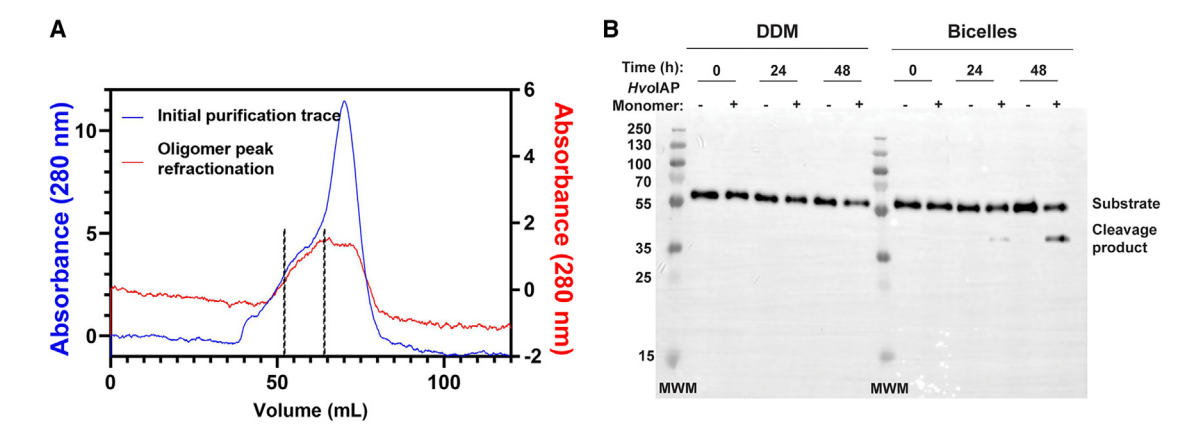


FIGURE 1 Purification and activity of h-HvoIAP. (A) Left, overlay of chromatogram for initial (blue) Sephacryl S-300 purification of h-HvoIAP and rerun (red) of oligomer peak (vertical dashed lines, 50–62 mL) showing some reequilibration to monomer. (B) Western blot of enzyme activity gel essay for h-HvoIAP monomer in DDM or bicelles toward fusion protein substrate ErbB4 (see materials and methods). No activity is observed at all time points for DDM, whereas a cleavage product is detected for the h-HvoIAP bicelle sample. MWM, molecular weight marker with masses in kDa as marked on the left side of the blot. Data shown are representative of at least two biological replicates. To see this figure in color, go online.

0.05% DDM consisted of a mixture of 0.028% DDM (Anatrace) and 0.022% $d_{25}\text{-DDM}$ (Anatrace). The sample, 14 mg/mL day-HvoIAP, was centrifuged at 16,100 $\times g$ for 15 min at 4°C and transferred to a 0.3 mL polypropylene vial and stored in the autosampler at a setpoint of 10°C. The SEC method was executed with an initial flow rate of 0.5 mL/min and subsequently decreased to 0.010 mL/min during elution. The outflow from the chromatography system was directed to a custom, demountable flow cell with a 1 mm pathlength for SANS data collection.

SANS data analysis and modeling

Azimuthally averaged and background corrected data were analyzed using established approaches for solution small-angle scattering. Initial SANS data analysis, including Guinier fits and pair-correlation, were performed using the BioXTAS RAW program and ATSAS suite (25,26). The pair distance distribution function P(r) was calculated using the indirect Fourier transform method implemented in the program GNOM (27). SANS data were fitted with the theoretical scattering profiles generated from the coordinates of atomic models using CRYSON (28). SANS data of HvoIAP monomer in DDM was used to perform ab initio shape reconstruction of the HvoIAP density map using DENSS software (www.tdgrant.com/denss/) (29). SANS data of HvoIAP monomer in bicelles was fitted with a cylinder model using the software SasView (version 5.0.4) (www.sasview.org/).

Molecular dynamics flexible fitting

AlphaFold2 within ColabFold (30) was used to generate a structural model for the *Hvo*IAP monomer, and then tetramer, based on its primary sequence. The model of the monomer was then improved using molecular dynamics flexible fitting (MDFF) (31). To balance the map-derived forces and those coming from the potential energy function, five different map-coupling strengths, referred to as G-scale, were considered. For four cases (G-scale-0.3, G-scale-0.2, G-scale-0.1, and G-scale-0.05), the additional map-derived force was applied to all residues except those in unstructured loops (primarily the acidic loop), each with a corresponding scaling factor of 0.3, 0.2, 0.1, and 0.05, respectively. In the fifth case (G-scale-0.1*), initially we applied the map-derived force to the entire protein with a scale factor of 0.2. After 1.25 ns, the resulting structure was used as the input for an additional 1.25 ns of MDFF while applying the map-derived force with a scale factor of 0.1 to structured residues only. All simulations were executed us-

ing NAMD (32) along with the CHARMM36m force field for proteins (33). The trajectory data generated from these simulations were further analyzed and visualized using visual molecular dynamics (34).

Transmission electron microscopy imaging

Negative stain grids were prepared by applying 3 μ L of 5% (w/w) empty bicelles, 2 μ M h-HvoIAP oligomers in DDM, or 2 μ M h-HvoIAP in the bicelle sample to CF400-Cu-TH grids (Electron Microscopy Sciences, Hatfield, PA). The sample was allowed to incubate on the grid for 1 min. Then the grid was side-blotted using a torn piece of Whatman no. 4 filter paper and washed by applying 3 μ L of ultrapure water to the grid, followed by incubation for 30 s. The grid was side blotted using a torn piece of Whatman no. 4 filter paper, stained with 3 μ L of 2% uranyl acetate, and incubated for 30 s. Excess uranyl acetate was removed by side-blotting, and the grid was air-dried for 2 min. Images were acquired at 120 kV using a JEOL JEM-1400 transmission electron microscope equipped with a Gatan OneView camera.

RESULTS

Fractionation and activity of HvoIAP

HvoIAP was identified in a bioinformatics study (9) as part of a search for new IAP orthologs that may provide new insight into this large enzyme family. HvoIAP is 32% identical in sequence to an experimentally characterized IAP from the methanogen MmIAP, UniProt: A3CWV0, GenBank: ABN 57850.1) and contains the catalytic motif YD ... GXGD, where X is typically a hydrophobic amino acid (Fig. S1). The main difference between HvoIAP and MmIAP is an acidic stretch of 33 residues in HvoIAP (N207-A140) that are absent in MmIAP, a feature that may be adaptive for the high salinity environment native to H. volcanii.

HvoIAP is recombinantly expressed in E. coli and purified at particularly high yield and purity. HvoIAP adopts two distinct species when purified using a Sephacryl S-300 column. One species overlaps with the elution fraction corresponding to the MmIAP monomer (35), and the

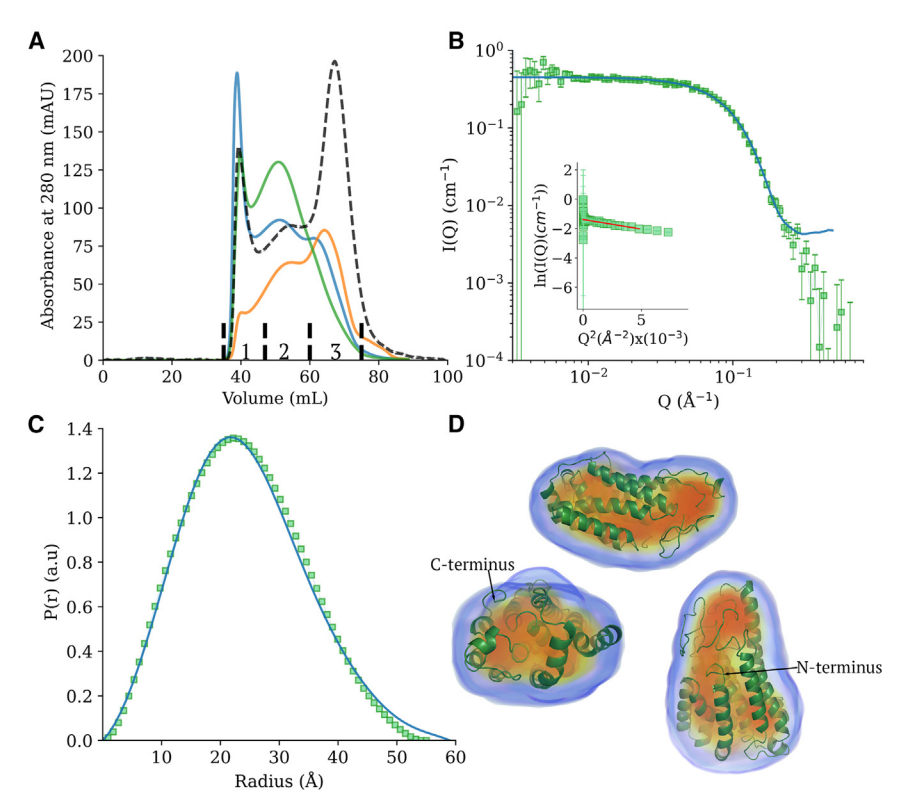


FIGURE 2 Purification of d-HvoIAP monomer in DDM and SANS with contrast-matched partially deuterated DDM/d25-DDM mixed micelles in 48.5% D₂O. (A) Comparison of SEC purification profile of d-HvoIAP to fractionated monomer and oligomer(s) species. Initial Sephacryl S-300 chromatogram trace of d-HvoIAP purification is shown as solid blue, the monomer polishing step is shown in orange, and the oligomer polishing step is shown as green. SEC fractions 1, 2, and 3 shown indicate the elution volumes for the void volume, oligomer, and monomer species, respectively. (B and C) SANS and P(r) profile for d-HvoIAP in DDM mixed micelles are shown as green squares. Error bars for SANS data are derived from counting statistics errors (N^{0.5}/N), where N is the number of detector counts. The inset shows the Guinier fit of d-HvoIAP monomer in DDM mixed micelles. The theoretical SANS and P(r) profile of the best MDFF model, based on the AlphaFold2 prediction, are shown as solid blue lines and overlaid with the experimental data. Error bars are $\sigma 1$ error (68% confidence level). (D) Three different views of a DENSS ab initio model of HvoIAP overlaid with the final model from MDFF (green) and are shown as rainbow shade (blue to red) and green colors, respectively. To see this figure in color, go online.

other is consistent with higher-order oligomer(s) (Fig. 1 A). The higher-ordered oligomer is at equilibrium with the monomer to some extent (Fig. 1 A). A survey of enzyme activity with substrates tested previously with MmIAP on either the monomer or oligomer fractions in DDM did not reproducibly yield detectable cleavage products (not shown). However, for a substrate derived from the tyrosine receptor kinase ErbB4 leader sequence, after reconstitution of the HvoIAP monomer into 5% DMPC/CHAPSO bicelles, a condition that enhances catalysis of MmIAP (36), a consistent cleavage band is observed (Fig. 1 B).

SANS contrast matching strategy

We followed the SANS strategy developed for deuterated MmIAP (d-MmIAP) (35). First, we suppressed the scattering contribution from detergent with a buffer containing 0.05% DDM composed of 44% (w/v) tail-deuterated DDM (d₂₅-DDM) with 56% (w/v) tail-protiated (non-deuterated) DDM. The partially deuterated DDM/d₂₅-DDM micelles have similar scattering length density for the micellar core and shell counterparts, resulting in near zero average scattering intensity across the Q-range studied. Second, the SANS experiments employed partially deuterated HvoIAP (d-HvoIAP), grown in 75% D₂O. Protiated protein has a typical neutron contrast match point of 42% D₂O, which is too close to the experimental conditions required for matching the mixed DDM/d₂₅-DDM micelles (48.5% D₂O), limiting the extent of signal possible from the protein. The partially deuterated d-HvoIAP corresponds to a match point around 80% D₂O (37). Like h-*Hvo*IAP, purified d-HvoIAP (Fig. S1 A) fractionates into an apparent oligomer and monomer (Fig. 2 A). When SEC is repeated, the monomer fractions reequilibrate to some extent into monomer and oligomer, whereas unlike h-HvoIAP (Fig. 1 A) the oligomer does not appear to reequilibrate to monomer.

Characterization of d-HvoIAP monomer in DDM by SANS

As in the previous work on MmIAP, the aforementioned contrast matching strategy successfully suppressed the detergent signal for the proposed d-HvoIAP monomeric fraction in DDM. SANS analysis indicates a radius of gyration (R_g) and maximum dimension (D_{max}) of 19.6 \pm 0.4 and 60 \pm 5 Å, respectively (inset, Fig. 2, B and C; Table 1). In addition, the pair-distance distribution function P(r) is symmetric, indicating a globular-shaped protein (Fig. 2 C), while the Kratky plot indicates a well-folded conformation in DDM micelles (Fig. S2 B). The molecular mass calculated by the Porod volume approach of the SANS data is 36.4 kDa, within 15% error of the calculated mass of HvoIAP (43 kDa). Overall, SANS data analysis supports the interpretation that this species is a monomer.

TABLE 1 Structural parameters of d-HvolAP monomer and oligomer studies using regular SANS and SEC-SANS compared with the MMIAP crystal structure (PDB: 4HYC)

	MmIAP monomer	MmIAP tetramer	d-HvoIAP monomer in DDM	d- <i>Hvo</i> IAP oligomer in DDM	d- <i>Hvo</i> IAP monomer in bicelles
(%) D ₂ O	_	_	48.5	48.5	15.0
I (0) (cm ⁻¹)	_	_	0.252 ± 0.003	0.053 ± 0.002	0.74 ± 0.02
R_a^{Guinier} (Å)	20.0	34.8	19.6 ± 0.4	69.8 ± 3.1	86.7 ± 3.4
R_g^{s} GNOM (Å)	20.4	34.4	18.9 ± 0.2	71.3 ± 2.7	104.3 ± 6.1
D _{max} (Å)	69.0	107	60 ± 5	225 ± 8	382 ± 30
MW ^{Porod} (kDa)	21.4	164.8	36.4	469	933
Porod volume (Å ³)	_	_	29,363.00	814,125.00	1,544,280.00
SEC-SANS of oligome	er in DDM				
	First peak	First tail	Second peak	Second tail	
$I(0) (cm^{-1})$	0.20 ± 0.02	0.14 ± 0.02	0.06 ± 0.01	_	
R_g^{GNOM} (Å)	136.7 ± 9.5	102.6 ± 9.6	92.8 ± 21.4	30.1 ± 6.1^{a}	

Error bars are $\sigma 1$ error (68% confidence level).

Structural modeling of the d-HvolAP monomer by combining SANS data with AlphaFold2 modeling

The crystal structure of MmIAP monomer (PDB: 4HYD, chain A) provides an acceptable fit to the SANS data, $\chi^2 = 1.9$ (Figs. S2 B and S3 A), and agrees well with the experimental pair distance distribution function, P(r)of HvoIAP (Fig. S3 B). In addition, ab initio shape reconstruction of *Hvo*IAP obtained using DENSS⁴² (Fig. S3 C) overlies reasonably well with the MmIAP crystal structure (PDB: 4HYD, chain A), particularly the position of the α helix N/C-terminus inside the envelope. However, two adjacent \(\alpha \) helices (residues proline 44 to proline 94 in MmIAP sequence) fall out of the SANS density map, and the model lacks residues L180 to R211 in MmIAP sequence, which are predicted to reside outside of the membrane.

To gain insight into differences between the MmIAP crystal structure and the SANS density shape model, we conducted MDFF (31) on an AlphaFold2 (38) model of the HvoIAP monomer generated using ColabFold (30), constrained by the SANS density map. In MDFF, forces to drive atoms into the density map are applied, in addition to those from the MD force field. Because the relatively low resolution of the density map does not allow for an unambiguous fit of the atomic model, different MDFF protocols were attempted to find the appropriate balance between the mapderived forces and those from the force field (see materials and methods). We selected a resulting model that represents the best compromise between maintaining secondary structure and achieving an optimal fit to the density map according to the cross-correlation coefficient; all fitted models are shown in Fig. S4. The starting AlphaFold2 model largely matches the MmIAP crystal structure model, particularly in the membrane helices (overall root mean-squared deviation ~ 1.5 Å, not shown). The configuration of the acidic loop (N207-A140), a region of low model confidence, is extended away from the membrane. A model of HvoIAP with the loop in an extended conformation, while fitting the SANS data to a reasonable degree ($\chi 2 = 3.42$), exhibits a longer D_{max} (70 Å). Our AlphaFold/MDFF model adjusts the acidic loop to a compact conformation adjoining the membrane and provides a good fit to the SANS data $(\chi 2 = 2.8, \text{ Fig. 2 B})$. The D_{max} of HvoIAP with the compact acidic loop is 60 Å, closely matching the experimentally determined value of 55 \pm 5 Å (Fig. 2 C). Finally, and in contrast to the two adjacent α helices in MmIAP crystal structure that were found outside of the SANS density, the HvoIAP AlphaFold/MDFF model fits well within the density map (Fig. 2 D). In sum, minor adjustments to the membrane helices combined with a compact acidic loop near the membrane match the SANS data better than the MmIAP crystal structure.

Characterization of d-HvoIAP high-order oligomers in DDM by SANS

The oligomeric fraction of d-HvoIAP was investigated next using SANS at the same contrast match condition as for the monomeric fraction (Fig. 3 A). SANS and P(r) analysis indicates the presence of elongated or rod-like structures of d-HvoIAP within the DDM environment (Fig. 3, A and B). In addition, SANS indicates an R_g of 69.8 \pm 3.1 Å for d-HvoIAP oligomer(s) in DDM (Fig. 3 A, inset; Table 1). To determine overall dimensions of these assemblies, we fit the data using a simple cylinder shape model with a fixed cylinder radius of 50 Å obtained from MmIAP crystal structure (PDB: 4HYC) and the fit indicates that d-HvoIAP oligomers adopt a length of 267 \pm 63 Å (Fig. 3) C). The P(r) analysis is consistent with a rod-like shape (Fig. 3 B), which in turn is consistent with the choice of the fit model, cylinder. The D_{max} obtained from the P(r) $(225 \pm 8 \text{ Å})$ agrees with the length determined by the cylinder model (267 \pm 63 Å) for these elongated d-HvoIAP oligomeric structures.

 $^{{}^{}a}R_{g}$ determined from the fit using a sphere model.

Thomas et al.

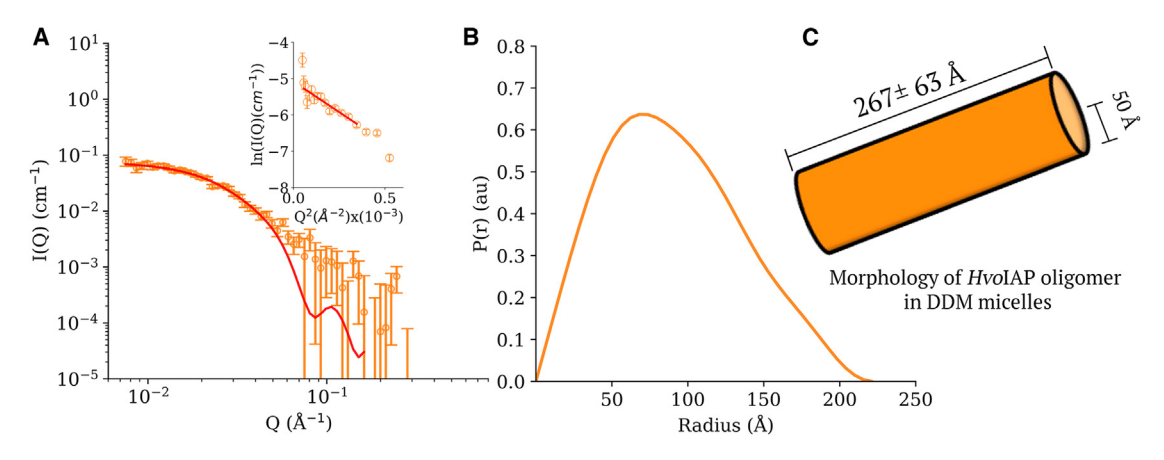


FIGURE 3 SANS analysis of d-HvoIAP oligomer in DDM. (A and B) SANS and P(r) profiles of d-HvoIAP oligomer in DDM micelles are shown as orange open circles and solid orange lines, respectively. The inset shows the Guinier fit of HvoIAP oligomer in DDM mixed micelles. Error bars for the morphological model and Guinier Fit are σ 1 error (68% confidence level), and for SANS data derived from counting statistics errors (N^{0.5}/N), where N is the number of detectors counts. The fit to SANS data of d-HvoIAP oligomer in DDM using a cylinder model is shown as a solid red line and overlaid on the experimental SANS data. (C) Morphological model of d-HvoIAP oligomer in DDM micelles. To see this figure in color, go online.

In-line SEC-SANS analysis of d-HvolAP oligomers in DDM

To further fractionate the species comprising the d-HvoIAP oligomers, we conducted a SANS experiment with in-line SEC, the first such experiment with a membrane protein at ORNL. After initial purification by Sephacryl S-300, we concentrated the pooled fractions of d-HvoIAP oligomers to 14 mg/mL and conducted SEC-SANS in continuous flow mode, as described in the materials and methods. During the SEC-SANS experiment, two prominent peaks were observed (Fig. 4).

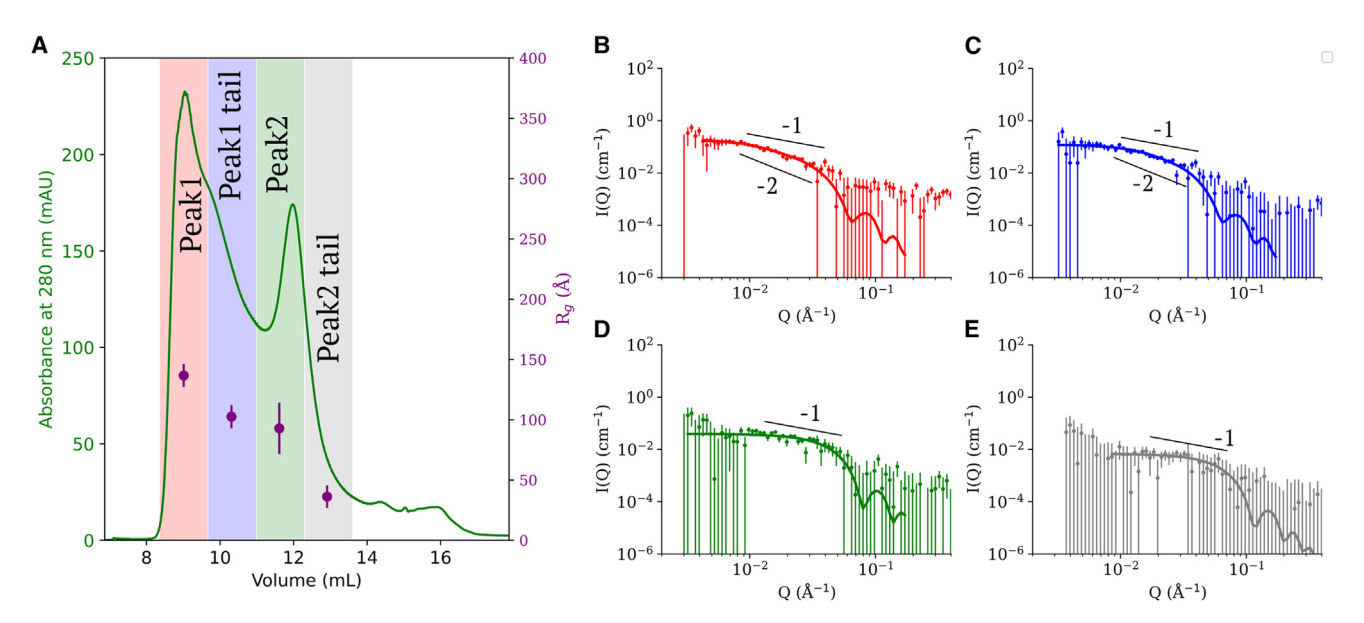


FIGURE 4 SEC-SANS analysis of d-HvoIAP oligomer in DDM. (A) SEC-SANS profile of polished oligomers studied at the contrast match point of DDM/ d₂₅-DDM mixed micelles (48% D₂O). The UV absorbance at 280 nm, depicted on the left-hand y axis, was recorded upstream of the SANS flow cell. To provide insight into the overall size variation of d-HvoIAP oligomers, we have plotted the radius of gyration (right-hand y axis) across the chromatogram. Each colored segment corresponds to a specific time slice during which SANS data was processed to obtain the SANS profiles shown in the Fig. S3. The gray segment represents the region where the smallest detectable d-HvoIAP oligomer was recorded in the SANS experiment. Error bars for radius of gyration are $\sigma 1$ error (68% confidence level). (B and C) SANS profile of the first peak and trailing tail colored as red and blue solid circles. (D and E) SANS profile of the second peak and last trailing tail colored as green and gray solid circles. The fit to SANS data of d-HvoIAP oligomer in micelles using a cylinder (B and C) and sphere (D and E) models are shown as solid lines and overlaid over the experimental SANS data. For (B)–(E), the slope in the mid-Q region for Peak 1, Peak 1 tail, and Peak 2 is between power law -1 and -2, indicating elongated shapes such as cylinders or wormlike chains, which have power law exponents in this range. Error bars for SANS data are derived from counting statistics errors $(N^{0.5}/N)$, where N is the number of detectors counts. To see this figure in color, go online.

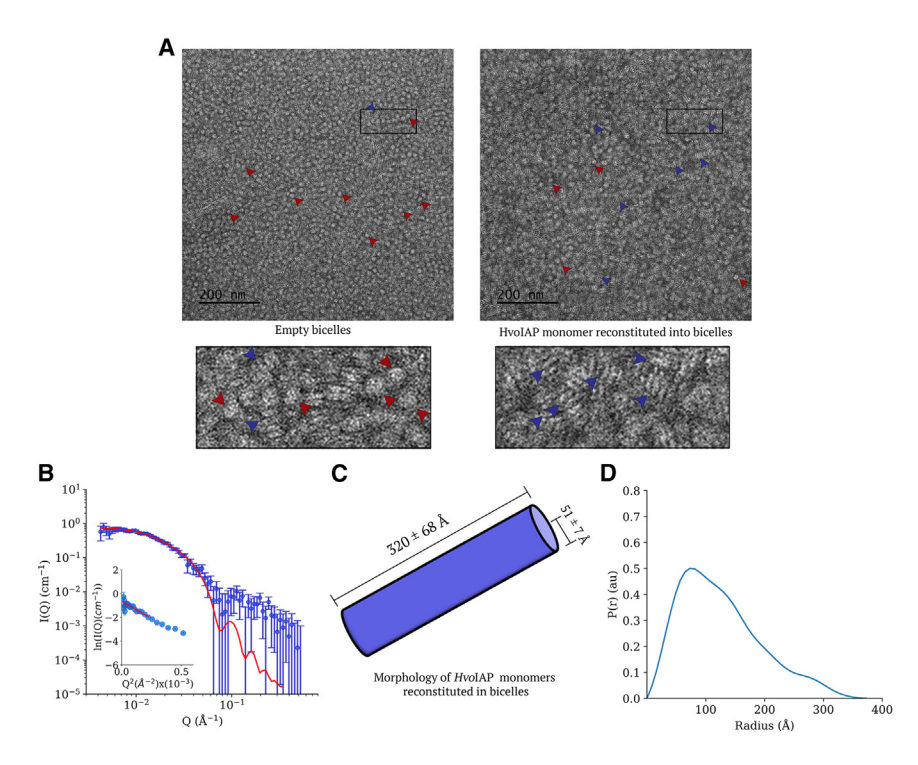


FIGURE 5 SANS analysis of d-HvoIAP oligomer in DMPC/CHAPSO bicelles. (A) Comparison of TEM image of empty bicelles in DDM buffer showing predominantly disc morphology (red) and bicelles after reconstitution with h-HvoIAP monomer showing predominantly ribbon morphology (blue). Samples were prepared on ice and then negatively stained and imaged at room temperature. Scale bars, 200 nm. Bicelle concentration is 5%, the same as used in SANS experiments, and d-HvoIAP concentration was 2 μ M. Bottom, zoom in from the box in the image above. (B) SANS profile of d-HvoIAP in bicelles shown as solid blue circles. The inset shows the Guinier fit of HvoIAP oligomer in bicelles. (C) Cylinder model of the HvoIAP oligomer in DMPC/CHAPSO bicelles. Error bars for Guinier Fit and morphological model are $\sigma 1$ error (68% confidence level), and for SANS data derived from counting statistics errors $(N^{0.5}/N)$, where N is the number of detectors counts. (D) P(r) profile of d-HvoIAP in bicelles. The fit to SANS data of d-HvoIAP oligomer in DMPC/CHAPSO bicelles using a cylinder model is shown as a solid red line and overlaid on the experimental SANS data. To see this figure in color, go online.

The first and major peak (red band) showed a wide elution profile with a trailing tail (purple band, Fig. 4, A–C), suggesting the coexistence of large d-HvoIAP oligomeric structures characterized by a similar overall size ($R_g = 136.7 \pm 9.5$ and $102.6 \pm 9.6 \,\mathrm{A}$, for the species at the peak and tail fractions, respectively) (insets of Fig. S5, A and B; Table 1). The scattering profiles of these d-HvoIAP oligomeric structures agreed with existence of elongated or rod-like structures previously observed in DDM micelles without in-line SEC (Figs. 4 B and S4 C). Fits using the cylinder model with a fixed radius of 50 Å indicate similar particle dimensions to one another, 480 ± 105 and 404 ± 69 Å for the peak and tail fractions, respectively. These d-HvoIAP structures are approximately 2-fold more elongated than the oligomeric species characterized using regular SANS measurements above without SEC (267 \pm 63 Å).

By contrast, in the second peak (green band), we observe species with scattering profiles that resemble a globular-like structure rather than a rod-like species (Fig. 4, D and E). In the early elution portion, we observe species with R_g of 92.8 \pm 21.4 Å (Fig. S5 C, inset; Table 1), and these data best fit a sphere model with radius of 56 \pm 4 Å. The P(r) profile of d-HvoIAP oligomers from SEC-SANS also indicates that the oligomers become more compact for species eluting in the Peak 1 tail and Peak 2 compared with that of eluting in the Peak 1 (Fig. S5 E). The data were also fit to a cylinder model, but we believe a sphere model is most appropriate because the SANS scattering profile shows limited features and the cylindrical model may represent overfitting. At the tail of the second peak (gray band), we observed d-HvoIAP assemblies with an R_g of 30.1 \pm 6.1 Å (Table 1). This R_g value was determined from the radius (38.9 \pm 7.9 Å) obtained through a sphere model fit to the scattering data (Fig. 4 B). Notably, this R_g value is close to the theoretical R_g (36 Å) determined for the crystal structure of the MmIAP tetramer (PDB: 4HYC, chains A-D), suggesting this d-HvoIAP assembly is likewise a tetramer.

Characterization of d-HvoIAP monomer reconstituted into DMPC/CHAPSO bicelles SANS reveals assembly to a higher-order oligomerization state

We reconstituted the purified d-HvoIAP monomer fraction in bicelles using established procedures (14) and minimized the scattering contribution of the bicelles with 15% D₂O, close to the contrast match point for the bicelles based on our previous study (39). In buffer containing 15% D₂O, we still observed a peak in the high-Q region due to differences in the SLD of tail and headgroup of DMPC. However, bicelles do not have appreciable scattering from the mid- to low-Q region of the entire Q range studied, confirming a good condition for contrast matching.

Transmission electron microscopy (TEM) images h-HvoIAP monomer reconstituted in bicelles, the condition under which activity was detected (Fig. 1 B), show extensive elongated ribbon-like species, distinct from the small disc-like species in the empty bicelles sample (Fig. 5 A). SANS data for d-HvoIAP monomer from SEC reconstituted in bicelles indicate an R_g of 89.2 \pm 5.6 Å (Fig. 5 B, inset; Table 1) and are best fit to a cylinder model with a length of 320 \pm 68 Å and a radius of 51 \pm 7 Å (Figs. 5 B and 3 C). This species has a radius consistent with MmIAP crystal structure and is about 1.5 times longer. The shape of these ribbons is consistent with elongated, worm-like lamellae morphology characterized by SANS beyond the phase transition temperature of \sim 22–23°C (39–41), and observed by TEM. In summary, d-HvoIAP monomer reconstituted into bicelles assembles into a higher-order species.

DISCUSSION

Neutron-based experiments are proving increasingly useful and accessible for the study of membrane protein structure and function. Our study represents the first in-line SEC-SANS experiment conducted on a membrane protein at ORNL, using a similar setup to that at the D22 beamline at the Institut Laue-Langevin (42,43). Thus far, SEC-SANS has enabled new insight into conformational changes adopted by membrane systems under different conditions relevant to function, generally large membrane proteins whose oligomeric state is already known (44,45). Smaller membrane proteins, such as HvoIAP, require different considerations for SANS than larger counterparts because any residual scattering from lipid or detergent components, which are of approximately the same size as the protein itself, contributes significantly to the overall signal, thus complicating interpretation. Resolving SANS data for small membrane proteins, with or without SEC, can be addressed with the assistance of complementary experiments (46,47) or, as we have, using a contrast matching strategy for the DDM tail and headgroup to extinguish the DDM signal combined with protein deuteration to enhance the signal in the SANS experiment (48).

In this study, we use SANS to reveal an interplay between the lipid environment and HvoIAP self-assembly. HvoIAP expression levels are the highest observed for any IAP, both in H₂O- and D₂O-containing media, a considerable advantage over MmIAP for SANS. The smaller HvoIAP species in DDM is a compact monomer similar to MmIAP. MDFF in combination with AlphaFold2 and constrained by the SANS data indicates some differences in HvoIAP as compared with MmIAP, particularly the acidic loop, which is not modeled in the experimental structure of MmIAP. Although nuances of the differences will require additional structures at higher resolution, it is tempting to posit that the acidic loop configuration in HvoIAP is stabilized by cations. The larger oligomer species purified in DDM appears as an elongated cylindrical rod-like species. Unexpectedly, upon reconstitution of HvoIAP into bicelles where enzyme activity was detected, SANS revealed that the monomers oligomerize to a rod-like species consistent with the high-temperature bicelle ribbon phase, which was further observed with TEM.

SEC-SANS enabled the oligomeric fraction of d-HvoIAP isolated from DDM to be probed in more detail than the bulk fractionation experiment initially conducted. Although the signal to noise of SEC-SANS was weaker overall, the data show that d-HvoIAP adopts assemblies of different sizes that are conservatively modeled as cylinders. At the tail end of the d-HvoIAP oligomer fraction is a somewhat more spherical species (\sim 10–20 nm in length and \sim 5 nm in height), similar to HvoIAP tetramers predicted de novo using AlphaFold2 and the tetrameric assembly seen in the asymmetric unit of the MmIAP crystal structure (PDB: 4HYC), all of which have dimensions of \sim 10 nm in diameter by \sim 4 nm in height. While an attractive interpretation of the data, we caution that the crystal structure arrangement cannot be unambiguously inferred from the SANS data.

Recently, using MmIAP, our lab reported that catalysis is sensitive to the lipid environment for numerous substrates. Namely, when the purified protein environment is changed from detergent (DDM) to 5% (w/w) DMPC/CHAPSO bicelles, cleavage is more precise (14) and there is a $3 \times$ increase in catalytic efficiency (36). This increase in catalysis is achieved in different ways. Depending on the substrate, the apparent affinity or maximal velocity is improved. Lipid-dependent oligomerization of HvoIAP is an attractive explanation for the changed activity observed in MmIAP as a function of lipid. In contrast to MmIAP, which has been studied for over a decade, HvoIAP is a new ortholog to be characterized and thus little is currently known. We detected enzymatic activity of HvoIAP most reproducibly for the monomer reconstituted into bicelles, suggesting that the elongated configuration of HvoIAP promoted by bicelles and observed by SANS underlies the activity and that this species is not misfolded HvoIAP due to, for example, overexpression in E. coli (49) or a mismatch in lipids (50). In the long term, the ability to triangulate lipid content and protein oligomerization alongside biological activity could lead to new ways to modulate IAP activity in space and time, in health and disease.

SUPPORTING MATERIAL

Supporting material can be found online at https://doi.org/10.1016/j.bpj. 2024.05.029.

AUTHOR CONTRIBUTIONS

Conceptualization, R.L.L.; methodology, G.M.T., Y.U., W.L., S.V.P., K.L.W., J.C.G., I.S.K., and V.S.U.; formal analysis, G.M.T., Y.U., W.L., S.V.P., and K.L.W.; investigation, G.M.T., Y.U., W.L., K.L.W., A.G., and G.G.; visualization, G.M.T., Y.U., and W.L.; writing – original draft, Y.U., W.L., V.S.U., and R.L.L.; writing – review & editing, K.L.W., J.C.G., I.S.K., V.S.U., and R.L.L.; supervision, J.C.G., I.S.K., V.S.U., and R.L.L.; funding acquisition, R.L.L.

ACKNOWLEDGMENTS

We acknowledge funding to R.L.L. from NSF MCB grant 1817796 and Georgia Institute of Technology COVID relief funds, to G.M.T. from the ACS Bridge Program and GAANN grant P200A210014, and to J.C.G. from NIH grant R01GM148586. We acknowledge the core facilities at the Parker H. Petit Institute for Bioengineering and Bioscience at the Georgia Institute of Technology for the use of their shared equipment, services, and expertise. This work benefited from the use of the SasView application, originally developed under NSF Award DMR-0520547. SasView contains code developed with funding from the European Union's Horizon 2020 research and innovation program under the SINE2020 Project, grant agreement no. 654000. Neutron scattering studies at the CG-3 Bio-SANS instrument at the High-Flux Isotope Reactor operated by the Oak Ridge National Laboratory were sponsored by the Office of Biological and Environmental Research and by the Scientific User Facilities Division, Office of Basic Energy Sciences, U.S. Department of Energy. This manuscript has been coauthored by UT-Battelle, LLC, under contract no. DE-AC05-401 00OR22725 with the U.S. Department of Energy. The United States Government retains, and the publisher, by accepting the article for publication, acknowledges that the United States 404 Government retains a nonexclusive, paid-up, irrevocable, worldwide license to publish or reproduce the published form of this manuscript, or allow others to do so, for United States Government purposes. The Department of Energy will provide public access to these results of federally sponsored research in accordance with the DOE Public Access Plan (http://energy.gov/downloads/doe-public-access-plan).

DECLARATION OF INTERESTS

The authors have no financial or other interests to disclose.

REFERENCES

- 1. Kuhnle, N., V. Dederer, and M. K. Lemberg. 2019. Intramembrane proteolysis at a glance: from signalling to protein degradation. J. Cell Sci. 132
- 2. Bai, X. C., C. Yan, ..., Y. Shi. 2015. An atomic structure of human gamma-secretase. Nature. 525:212-217.
- 3. Nyborg, A. C., L. Herl, ..., T. E. Golde. 2006. Signal peptide peptidase (SPP) dimer formation as assessed by fluorescence lifetime imaging microscopy (FLIM) in intact cells. Mol. Neurodegener. 1:16.
- 4. Nyborg, A. C., A. Y. Kornilova, ..., T. E. Golde. 2004. Signal peptide peptidase forms a homodimer that is labeled by an active site-directed gamma-secretase inhibitor. J. Biol. Chem. 279:15153-15160.
- 5. Cerevantes, S., C. A. Saura, ..., G. Marfany. 2004. Functional implications of the presenilin dimerization: reconstitution of gamma-secretase activity by assembly of a catalytic site at the dimer interface of two catalytically inactive presenilins. J. Biol. Chem. 279:36519–36529.
- 6. Li, X., S. Dang, ..., Y. Shi. 2013. Structure of a presentilin family intramembrane aspartate protease. Nature. 493:56-61.
- 7. Miyashita, H., Y. Maruyama, ..., T. Iwatsubo. 2011. Three-dimensional structure of the signal peptide peptidase. J. Biol. Chem. 286:26188-26197.
- 8. Schrul, B., K. Kapp, ..., B. Dobberstein. 2010. Signal peptide peptidase (SPP) assembles with substrates and misfolded membrane proteins into distinct oligomeric complexes. Biochem. J. 427:523-534.
- 9. Raut, P., J. B. Glass, and R. L. Lieberman. 2021. Archaeal roots of intramembrane aspartyl protease siblings signal peptide peptidase and presenilin. Proteins. 89:232-241.
- 10. Chen, C. Y., N. S. Malchus, ..., M. K. Lemberg. 2014. Signal peptide peptidase functions in ERAD to cleave the unfolded protein response regulator XBP1u. *EMBO J.* 33:2492–2506.

- 11. Escamilla-Ayala, A. A., R. Sannerud, ..., W. Annaert. 2020. Super-resolution microscopy reveals majorly mono- and dimeric presenilin1/ gamma-secretase at the cell surface. Elife. 9.
- 12. Sanders, C. R., and G. C. Landis. 1995. Reconstitution of membrane proteins into lipid-rich bilayered mixed micelles for NMR studies. Biochemistry. 34:4030-4040.
- 13. Breyton, C., F. Gabel, ..., C. Ebel. 2013. Small angle neutron scattering for the study of solubilised membrane proteins. Eur. Phys. J. E Soft
- 14. Naing, S. H., S. Kalyoncu, ..., R. L. Lieberman. 2018. Both positional and chemical variables control in vitro proteolytic cleavage of a presenilin ortholog. J. Biol. Chem. 293:4653-4663.
- 15. Naing, S. H., K. M. Vukoti, ..., R. L. Lieberman. 2015. Catalytic Properties of Intramembrane Aspartyl Protease Substrate Hydrolysis Evaluated Using a FRET Peptide Cleavage Assay. ACS Chem. Biol. 10:2166-2174.
- 16. Ujwal, R., and J. U. Bowie. 2011. Crystallizing membrane proteins using lipidic bicelles. Methods. 55:337-341.
- 17. Gasteiger, E., C. Hoogland, ..., A. Bairoch. 2005. Protein Identification and Analysis Tools on the ExPASy Server. Humana Press, pp. 571-607.
- 18. Marley, J., M. Lu, and C. Bracken. 2001. A method for efficient isotopic labeling of recombinant proteins. J. Biomol. NMR. 20:71-75.
- 19. Tornkvist, M., G. Larsson, and S. O. Enfors. 1996. Protein release and foaming in Escherichia coli cultures grown in minimal medium. Bioprocess Eng. 15:231-237.
- 20. Holme, T., S. Arvidson, ..., B. Pavlu. 1970. Enzymes: Laboratory-Scale Production. Process Biochem. 5:62-66.
- 21. Heller, W. T. 2010. Small-angle neutron scattering and contrast variation: a powerful combination for studying biological structures. Acta Crystallogr D Struct Biol. 66:1213–1217.
- 22. Heller, W. T., V. S. Urban, ..., D. A. Myles. 2014. The Bio-SANS instrument at the High Flux Isotope Reactor of Oak Ridge National Laboratory. J. Appl. Crystallogr. 47:1238-1246.
- 23. Yao, X., B. Avery, ..., K. Vodopivec. 2021. A Unified User-Friendly Instrument Control and Data Acquisition System for the ORNL SANS Instrument Suite. Appl. Sci. 11:1216.
- 24. Arnold, O., J. C. Bilheux, ..., J. Zikovsky. 2014. Mantid—Data analysis and visualization package for neutron scattering and μ SR experiments. Nucl. Instrum. Methods Phys. Res. B. 764:156-166.
- 25. Franke, D., M. V. Petoukhov, ..., D. I. Svergun. 2017. ATSAS 2.8: a comprehensive data analysis suite for small-angle scattering from macromolecular solutions. J. Appl. Crystallogr. 50:1212–1225.
- 26. Hopkins, J. B., R. E. Gillilan, and S. Skou, 2017. BioXTAS RAW: improvements to a free open-source program for small-angle X-ray scattering data reduction and analysis. J. Appl. Crystallogr. 50:1545–1553.
- 27. Svergun, D. I. 1992. Determination of the regularization parameter in indirect-transform methods using perceptual criteria. J. Appl. Crystallogr. 25:495-503.
- 28. Svergun, D., C. Barberato, and M. H. J. Koch. 1995. CRYSOL a Program to Evaluate X-ray Solution Scattering of Biological Macromolecules from Atomic Coordinates. J. Appl. Crystallogr. 28:768–773.
- 29. Grant, T. D. 2018. Ab initio electron density determination directly from solution scattering data. Nat. Methods. 15:191-193.
- 30. Mirdita, M., K. Schütze, ..., M. Steinegger. 2022. ColabFold: making protein folding accessible to all. Nat. Methods. 19:679-682.
- 31. Trabuco, L. G., E. Villa, ..., K. Schulten. 2008. Flexible fitting of atomic structures into electron microscopy maps using molecular dynamics. Structure. 16:673-683.
- 32. Phillips, J. C., D. J. Hardy, ..., E. Tajkhorshid. 2020. Scalable molecular dynamics on CPU and GPU architectures with NAMD. J. Chem. Phys. 153:044130.
- 33. Huang, J., S. Rauscher, ..., A. D. MacKerell, Jr. 2017. CHARMM36m: an improved force field for folded and intrinsically disordered proteins. Nat. Methods. 14:71-73.

- 34. Humphrey, W., A. Dalke, and K. Schulten. 1996. VMD: visual molecular dynamics. J. Mol. Graph. 14:27-38.
- 35. Naing, S. H., R. C. Oliver, ..., R. L. Lieberman. 2018. Solution Structure of an Intramembrane Aspartyl Protease via Small Angle Neutron Scattering. *Biophys. J.* 114:602–608.
- 36. Wu, Y., G. M. Thomas, ..., R. L. Lieberman. 2023. Lipid environment modulates processivity and kinetics of a presenilin homolog acting on multiple substrates in vitro. J. Biol. Chem. 299:105401.
- 37. Weiss, K. L., Y. Fan, ..., H. O'Neill. 2021. Fed-batch production of deuterated protein in Escherichia coli for neutron scattering experimentation. Methods Enzymol. 659:219-240.
- 38. Jumper, J., R. Evans, ..., D. Hassabis. 2021. Highly accurate protein structure prediction with AlphaFold. Nature. 596:583-589.
- 39. Leite, W. C., Y. Wu, ..., V. S. Urban. 2022. Change in Morphology of Dimyristoylphosphatidylcholine/Bile Salt Derivative Bicelle Assemblies with Dodecylmaltoside in the Disk and Ribbon Phases. J. Phys. Chem. Lett. 13:9834-9840.
- 40. Sharma, V. K., E. Mamontov, ..., V. Urban. 2015. Nanoscopic dynamics of phospholipid in unilamellar vesicles: effect of gel to fluid phase transition. J. Phys. Chem. B. 119:4460-4470.
- 41. Li, M., H. H. Morales, ..., M.-P. Nieh. 2013. Morphological Characterization of DMPC/CHAPSO Bicellar Mixtures: A Combined SANS and NMR Study. Langmuir. 29:15943-15957.
- 42. Johansen, N. T., M. C. Pedersen, ..., L. Arleth. 2018. Introducing SEC-SANS for studies of complex self-organized biological systems. Acta Crystallogr. D Struct. Biol. 74:1178-1191.

- 43. Martel, A., C. Cocho, ..., L. Porcar. 2023. Upgraded D22 SEC-SANS setup dedicated to the biology community. J. Appl. Crystallogr. 56:994-1001.
- 44. Lycksell, M., U. Rovšnik, ..., E. Lindahl. 2022. Biophysical characterization of calcium-binding and modulatory-domain dynamics in a pentameric ligand-gated ion channel. Proc. Natl. Acad. Sci. USA. 119:e2210669119.
- 45. Johansen, N. T., M. Bonaccorsi, ..., L. Arleth. 2022. Mg(2+)-dependent conformational equilibria in CorA and an integrated view on transport regulation. Elife. 11:e71887.
- 46. Combet, S., F. Bonneté, ..., J. J. Lacapère. 2023. Effect of amphiphilic environment on the solution structure of mouse TSPO translocator protein. Biochimie. 205:61-72.
- 47. Kassem, N., R. Araya-Secchi, ..., B. B. Kragelund. 2021. Order and disorder-An integrative structure of the full-length human growth hormone receptor. Sci. Adv. 7, eabh3805.
- 48. Oliver, R. C., S. V. Pingali, and V. S. Urban. 2017. Designing mixed detergent micelles for uniform neutron contrast. J. Phys. Chem. Lett. 8:5041-5046.
- 49. Wagner, S., L. Baars, ..., J. W. de Gier. 2007. Consequences of membrane protein overexpression in Escherichia coli. Mol. Cell. Proteomics. 6:1527-1550.
- 50. Torreblanca, M., F. Rodriguez-Valera, ..., M. Kates. 1986. Classification of non-alkaliphilic halobacteria based on numerical taxonomy and polar lipid composition, and description of Haloarcula gen. nov. and Haloferax gen. nov. Syst. Appl. Microbiol. 8:89-99.